ChemPubSoc Europe

DOI: 10.1002/cphc.201200931

Nanocavity-Based Determination of Absolute Values of Photoluminescence Quantum Yields

Alexey I. Chizhik,*[a] Ingo Gregor,[a] Benedikt Ernst,[b] and Jörg Enderlein*[a]

We present a new method for determining absolute values of quantum yield of luminescent emitters, which is based on the modification of the radiative transition of emitters within a tunable metallic nanocavity. The method presented is easy to set up and works without any calibration. It will thus be useful for all applications where absolute and calibration-free measurements of luminescence quantum yields are needed. Moreover, it requires only a minute amount of low-concentration fluorophore solution. We give a detailed description of the theory and data evaluation of the nanocavity measurements, and report experimental results for several common dyes in aqueous solution.

1. Introduction

Of all the photophysical parameters of a luminescent emitter (absorption cross section or extinction, emission spectrum, excited state lifetime, etc.), the quantum yield (QY) of emission is one of the most difficult to assess. The QY is a measure of the conversion efficiency of absorbed light into emitted photons, and is thus a key parameter of its photophysics.[1] It determines the suitability of luminescent compound for application in light-emitting diodes,[2] single-photon sources,[3] solar cells,[4] laser technology,[5] or labeling of biological samples.[6]

The era of quantitative QY measurements began in 1924 with Vavilov's invention of the first reliable method for measuring the absolute luminescence efficiency in solution by comparing the luminescent emission with scattering intensities.[7] Nowadays, the QY is most often determined in a comparative manner by measuring the total luminescence emission intensity against that of a fluorescent standard of known QY[8–11] or against the scattering intensity of a non-luminescent scatterer.[13] Another way to determine the QY is to measure the thermal power released after excitation in a so-called thermal lensing measurement.[12,13] This method provides one of the most accurate ways to determine the QY, but it is technically challenging and requires large sample concentrations. Finally, the photoluminescence QY value can be obtained directly by measuring the number of emitted photons per number of photons absorbed by a sample using an integrating sphere setup.[14,15] While this technique avoids inaccuracies typically occurring when performing referential measurements of QY, its precision relies on the correct radiometric characterization of the integration sphere setup and on the proper account of reabsorption effects.[15]

In general, the QY can be defined as the ratio of the radiative (k_r) to the non-radiative (k_{nr}) transition rate from the excited to the ground state of an emitter [Eq. (1)]:

$$\Phi = k_r/(k_r + k_{nr}) \quad (1)$$

Thus, if one would be able to specifically vary either the radiative or non-radiative transition rate while measuring the total deexcitation rate $k_r + k_{nr}$ (inverse excited state lifetime), one could also deduce the value of the QY of an emitter. In recent years, several publications have dealt with the controlled modification of the radiative transition rate of an emitter by tuning the local density of states (LDOS) of the electromagnetic field at its position. As was pointed out by Purcell, by changing the LDOS of the electromagnetic field, one changes the coupling of an emitter's excited-to-ground-state transition to that field, thus leading to a modification of the radiative transition rate.[16] This so-called Purcell effect has been measured for fluorophores placed between two gold nanoparticles,[17] close to a dielectric interface,[19,18] a metallic mirror,[20–22] or a sharp tip of a scanning probe microscope.[23,24] An efficient way of changing the LDOS of the electromagnetic field is to embed an emitter into a plane-parallel optical resonator,[25–30] which allows for precise control of the LDOS by varying the cavity length. Moreover, this length can be precisely monitored by measuring the cavity's transmission spectrum, which eliminates potential systematic errors caused by mechanical instabilities of the system. We have recently employed such a tunable cavity to measure the QY of single molecules at fixed positions inside the resonator,[28] and for investigating the impact of rotational diffusion on the electrodynamic coupling of dipole emitters to the cavity modes.[30]

Here, we apply the tunable nanocavity for the absolute, calibration-free measurement of QY values of fluorophores in solu-

[a] Dr. A. I. Chizhik, Dr. I. Gregor, Prof. Dr. J. Enderlein
III. Institute of Physics
Georg August University
37077 Göttingen (Germany)
E-mail: chizhik@physik3.gwdg.de
enderlein@physik3.gwdg.de

[b] B. Ernst
Institute of Material Physics
Georg August University
37077 Göttingen (Germany)

tion. The core idea of the nanocavity-based method is to measure the change of the fluorescence lifetime of a solution of fluorophores inside a planar metal nanocavity as a function of cavity length. Changing the cavity length changes the LDOS inside the cavity and thus the radiative transition rate of the enclosed fluorophores.[31] Employing a complete and quantitative theoretical model of the expected change of k_r as a function of cavity length, and knowing the full excited-to-ground state transition rate $k_r + k_{nr}$ from the lifetime measurement, one can use Equation (1) for fitting an absolute value of the QY. As will be shown below, this kind of measurement is easy to set up, yields an absolute and reference-free value of the QY, and needs only minute amounts of sample (microliters of micromolar or less concentration). Thus, the method will be of considerable interest for all applications where rapid and absolute QY measurements on small sample quantities are required.

2. Theory

A necessary prerequisite for successfully using the cavity-modulated lifetime for accurate QY measurements is an accurate theoretical understanding of the underlying physics. This section gives a detailed description of the theoretical model which is employed for the data evaluation of the measurements. Readers who are not interested in the details of the theoretical model can skip this part and can go directly to the experimental section.

The theoretical treatment is divided into several steps. First, one has to calculate the electric field distribution within the cavity as generated by the focused laser beam. Second, the electromagnetic coupling of the dipole emission to the cavity is considered. Third, the molecule detection function (MDF), that is, the efficiency to detect a photon from an emitting molecule at a given position and with a given orientation has to be determined. In a last step, all this information is used to obtain the measured average lifetime as a function of cavity length.

2.1. Electric Field Distribution of Excitation Light

The electromagnetic field distribution inside the cavity is calculated following the concept of Wolf and Richards.[32,33] The core idea is to expand the electric field of the focused laser light into a superposition of plane waves, and then to calculate the interaction of each plane wave component with the cavity. It is assumed that the experiment is performed close to diffraction-limited focusing so that the electric field of the excitation light in the back focal plane of the objective is approximated by a linearly polarized plane wave. The excitation geometry is shown in Figure 1. At each position of the back-aperture of the focusing objective, the electric field vector of the incoming, linearly polarized electromagnetic plane wave is separated into the radial ($\mathbf{E}_p$) and tangential ($\mathbf{E}_s$) components. Each component is then traced separately from the outside to the inside of the cavity using Fresnel's transmission coefficients for plane waves incident on planar surfaces. A more detailed depiction

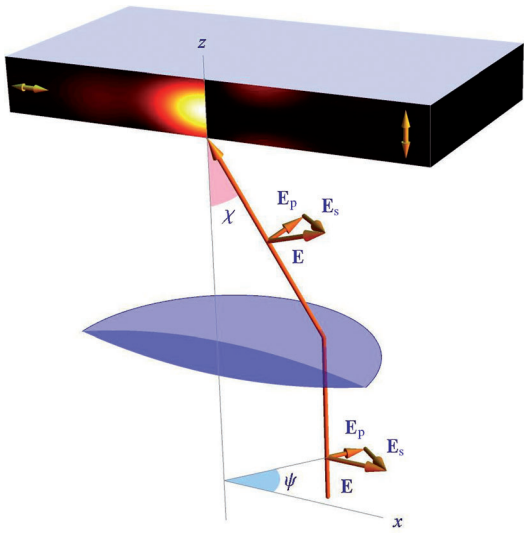

Figure 1. Geometry of excitation. A plane wave with linear polarization along the *x*-axis is focused by the objective lens onto the bottom of the cavity. The path and polarization for one plane wave component incident under an angle χ on the cavity is shown. During the calculation of the excitation intensity distribution inside the cavity, one has to decompose the *x* polarization of each incident plane wave into its *p*- and *s*-polarized parts ($\mathbf{E}_p$ and $\mathbf{E}_s$, respectively), which are transmitted into the cavity with different transmission coefficients. The density plots in the cavity show cross-sections of the excitation intensity for a horizontally aligned (left side) and for a vertically aligned (right side) excitation dipole. For these calculations, it was assumed that the cavity has an inner height of 200 nm and consists of two silver mirrors of 30 nm (bottom) and 60 nm (top) thickness, and that the cavity-filling solvent is water. The objective was assumed to be a water-immersion objective with 1.2 numerical aperture, focusing a plane *x*-polarized wave onto the bottom of the cavity.

of the geometry of the involved plane waves and all vectors is given in Figure 2. Each plane-wave component incident on the cavity under an angle χ is coupled to two plane waves inside the cavity traveling under an angle χ_m, one propagating upwards and the second downwards. The angles χ and χ_m are connected by Snell's law of refraction, $n\sin\chi = n_m\sin\chi_m$, where *n*

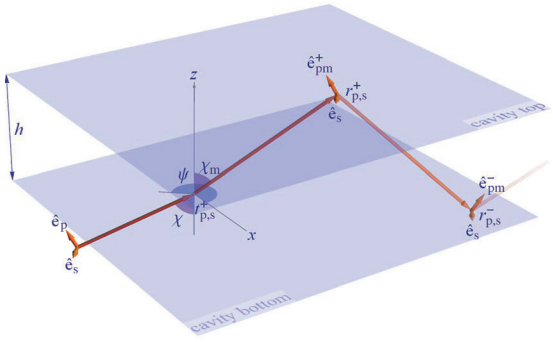

Figure 2. Visualization of vectors and angles as used in the calculation of the excitation intensity distribution. The action of one single plane wave incident onto the cavity from below from a direction defined by polar angle χ and azimuthal angle ψ is depicted. Generally, the plane wave has *p*- and *s*-polarized components along unit vectors $\hat{\mathbf{e}}_p$ and $\hat{\mathbf{e}}_s$, respectively. The plane wave is transmitted through the bottom of the cavity, giving rise to plane waves traveling under angles $\pm\chi_m$ inside the cavity. The multiple reflections of the plane waves inside the cavity, with reflection coefficients $r_{p,s}^{+}$ at the top and $r_{p,s}^{-}$ at the bottom of the cavity are also indicated.

is the refractive index of the objective's immersion medium, and n_m is the refractive index of the solution. When integrating over all polar and azimuthal incidence angles, the electric field distribution is given, up to an overall constant, by Equation (2):

$$\begin{aligned} E_x(\rho,\phi,z) &= f_0(\rho,z) + f_2(\rho,z)\cos 2\phi \\ E_y(\rho,\phi,z) &= f_2(\rho,z)\sin 2\phi \\ E_z(\rho,\phi,z) &= f_1(\rho,z)\cos\phi \end{aligned} \tag{2}$$

where (ρ,ϕ,z) are cylindrical coordinates, with z along the optical axis and perpendicular to the cavity's surfaces. It is assumed that the excitation light is polarized along the axis $\phi = 0$. The functions $f_{0,1,2}(\rho,z)$ are independent on the angular coordinate ϕ and are given by integrating over all plane wave components of the focused laser field as Equation (3):

$$f_j = \int_0^{\chi_0} d\chi \sin\chi \sqrt{\cos\chi} J_n(k_m \sin\chi_m \rho) \left[\kappa_j^+(\chi_m) e^{ik_m z\cos\chi_m} + \kappa_j^-(\chi_m) e^{-ik_m z\cos\chi_m}\right] \tag{3}$$

The integration variable χ runs from zero up to its maximum value $\chi_0 = \arcsin(n/\mathrm{NA})$ determined by the numerical aperture NA of the objective. k_m denotes the length of the wave vector within the solvent inside the cavity. J_α denotes cylindrical Bessel functions of the first kind. The quantities $\kappa_j^{\pm}$ are angle-dependent coefficients given by Equation (4):

$$\begin{aligned} \kappa_0^{\pm}(\chi_m) &= T_s^{\pm}(\chi_m)\cos\chi_m + T_p^{\pm}(\chi_m) \\ \kappa_1^{\pm}(\chi_m) &= -2iT_s^{\pm}(\chi_m)\sin\chi_m \\ \kappa_2^{\pm}(\chi_m) &= -T_s^{\pm}(\chi_m)\cos\chi_m + T_p^{\pm}(\chi_m) \end{aligned} \tag{4}$$

where $T_s^{\pm}$ and $T_p^{\pm}$ are effective transmission coefficients (from objective into the cavity) for plane s and p waves. The plus and minus superscripts refer to plane waves propagating in the forward (towards increasing z values) and backward (towards decreasing z values) direction, respectively. These coefficients are given by Equation (5):

$$T_{p,s}^{+} = \frac{t_{p,s}^{+}}{1 - r_{p,s}^{+} r_{p,s}^{-} e^{2iw_m h}} \tag{5}$$

and Equation (6):

$$T_{p,s}^{-} = \frac{t_{p,s}^{+} r_{p,s}^{+} e^{2iw_m h}}{1 - r_{p,s}^{+} r_{p,s}^{-} e^{2iw_m h}} \tag{6}$$

where w_m is the absolute value of the z component of the wave vector inside the cavity, $t_{p,s}^{+}$ is Fresnel's transmission coefficients for plane p and s waves from the outside to the inside at the bottom of the cavity, respectively, and $r_{p,s}^{\pm}$ is Fresnel's reflection coefficients for plane p and s waves at the top (superscript $+$) and bottom (superscript $-$) of the cavity, respectively, see also Figure 2. $t_{p,s}^{+}$ and $r_{p,s}^{\pm}$ are found in a standard way with the help of a transfer-matrix approach.[36,37] It should be noted that here the optical properties of the metal films are contained in the calculations. Equations (5) and (6) take into account all possible multiple reflections of the plane wave components inside the cavity.

Knowing the electric field distribution inside the cavity, the excitation rate of a molecule with position $\{\rho,\phi,z\}$ and absorption dipole moment $\mathbf{p}$ is proportional to $|\mathbf{p}\cdot\mathbf{E}^2|$ (neglecting any non-linear saturation effects). For the evaluation of the cavity experiments, we need the excitation rate only as a function of the angle θ between the molecule's dipole axis and the optical axis, thus averaging the dipole orientation over the azimuthal angle around the optical axis. Using the above equations, this excitation rate, $I(\theta)$, is then given by Equation (7):

$$I(\theta) = I_\perp \cos^2\theta + I_\parallel \sin^2\theta \tag{7}$$

with [Eq. (8)]:

$$\begin{aligned} I_\perp(\rho,\phi,z) &= 1/2\,(|E_x(\rho,\phi,z)|^2 + |E_y(\rho,\phi,z)|^2) \\ I_\parallel(\rho,\phi,z) &= |E_z(\rho,\phi,z)|^2 \end{aligned} \tag{8}$$

As an example, Figure 1 shows the calculated excitation intensity distribution generated when focusing a plane wave through a water-immersion objective with 1.2 N.A. onto a water-filled cavity consisting of two silver mirrors with bottom and top thickness values of 30 and 60 nm, respectively, and a cavity height of 200 nm at an excitation wavelength of 640 nm.

2.2. Coupling of Dipole Emission to Cavity

The electric field generated by an electric dipole oscillator with orientation vector $\mathbf{p}$ at position $\rho = 0$ and $z = z_m$ in unbounded space filled with solvent of refractive index n can be written as a superposition of plane waves in the Weyl representation[34,35] and reads (up to some constant pre-factor) as Equation (9):

$$\mathbf{E}_0(\mathbf{\rho}, z) = \int\int \frac{d\mathbf{q}}{w_m} \left[\mathbf{e}_p^{\pm}\left(\mathbf{e}_p^{\pm}\cdot\mathbf{p}\right) + \mathbf{e}_s(\mathbf{e}_s\cdot\mathbf{p})\right] e^{i\mathbf{q}\cdot\mathbf{\rho} + iw_m|z - z_m|} \tag{9}$$

where $\mathbf{q}$ is the part of the wave vector perpendicular to the optical axis, and $w_m = \sqrt{k_m^2 - q^2}$ is its z-component; k_0 and k_m are the length of the wave vectors in vacuum and in solvent, respectively. The unit vectors $\mathbf{e}_p^{\pm}$ and $\mathbf{e}_s$ are pointing along the electric field polarization of p and s waves, respectively, as shown in Figure 3, where the plus sign applies for $z > z_m$, and the minus sign for $z < z_m$. The integration over $\mathbf{q}$ extends over the whole two-dimensional $\mathbf{q}$ plane. When solving Maxwell's equations for the cavity with the field $\mathbf{E}_0$ as source term, the total electric field inside the cavity can be written in a similar plane wave representation [Eq. (10)]:

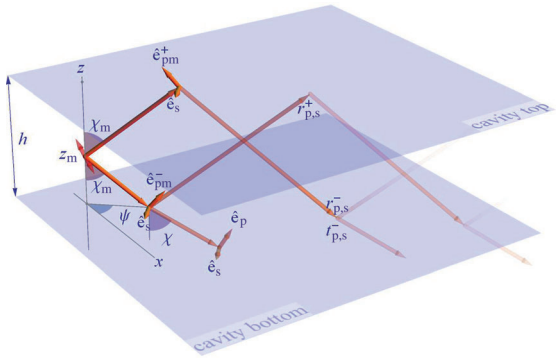

Figure 3. Visualization of vectors and angles used for the calculation of the emission of an electric dipole which is indicated by the red double-arrow at positions z_m above the cavity bottom. The emitted field can be represented by a superposition of plane waves. Plane wave components traveling along polar angles $\pm\chi_m$ and azimuthal angle ψ inside the cavity are shown. After passing the bottom of the cavity, they give rise to plane waves traveling towards the objective (negative z direction) under an angle χ with respect to the optical axis.The multiple reflections of the plane waves inside the cavity, again with reflection coefficients $r_{p,s}{}^{+}$ at the top and $r_{p,s}{}^{-}$ at the bottom are also indicated.

$$\begin{aligned}\mathbf{E}(\boldsymbol{\rho},z) = \mathbf{E}_0(\boldsymbol{\rho},z) + \iint \frac{d\mathbf{q}}{w_m}\Big\{ &\mathbf{e}_p^- \left[\left(R_p^{--}\mathbf{e}_p^- + R_p^{-+}\mathbf{e}_p^+\right)\cdot\mathbf{p}\right] e^{-iw_m z} \\ &+\mathbf{e}_p^+ \left[\left(R_p^{++}\mathbf{e}_p^+ + R_p^{+-}\mathbf{e}_p^-\right)\cdot\mathbf{p}\right] e^{iw_m z} \\ &+\mathbf{e}_s^- \left[\left(R_s^- e^{-iw_m z} + R_s^+ e^{iw_m z}\right)\mathbf{e}_s\cdot\mathbf{p}\right]\Big\} e^{i\mathbf{q}\cdot\boldsymbol{\rho}}\end{aligned} \tag{10}$$

where $R_p{}^{\pm\pm}$and $R_s{}^{\pm}$are q-dependent cumulative reflection coefficients for plane p and s waves which are given by Equation (11):

$$\begin{aligned} R_p^{--} &= \frac{r_p^+ r_p^- e^{iw_m(2h+z_m)}}{1 - r_p^+ r_p^- e^{2iw_m h}}, \quad R_p^{-+} = \frac{r_p^+ e^{iw_m(2h-z_m)}}{1 - r_p^+ r_p^- e^{2iw_m h}} \\ R_p^{++} &= \frac{r_p^+ r_p^- e^{iw_m(2h-z_m)}}{1 - r_p^+ r_p^- e^{2iw_m h}}, \quad R_p^{+-} = \frac{r_p^- e^{iw_m z_m}}{1 - r_p^+ r_p^- e^{2iw_m h}} \end{aligned} \tag{11}$$

and Equation (12):

$$\begin{aligned} R_s^- &= \frac{r_s^+ r_s^- e^{iw_m(2h+z_m)} + r_s^+ e^{iw_m(2h-z_m)}}{1 - r_s^+ r_s^- e^{2iw_m h}} \\ R_s^+ &= \frac{r_s^+ r_s^- e^{iw_m(2h-z_m)} + r_s^- e^{iw_m z_m}}{1 - r_s^+ r_s^- e^{2iw_m h}} \end{aligned} \tag{12}$$

Equations (2)–(6) take into account all multiple reflections of the plane-wave components inside the cavity. The integration in Equation (2) extends over the whole **q** plane, and as soon as the length of the **q** vector becomes larger than the wave vector length k_m, the integral starts to sum over all possible evanescent wave components, thus taking full account of the near-field interaction of the emitter with the cavity.

The magnetic field is derived from $\mathbf{E}(\boldsymbol{\rho},z)$ by employing Faraday's law of induction, Equation (13):

$$\mathbf{B}(\rho,z) = -ik_0{}^{-1}\mathbf{rotE}(\rho,z) \tag{13}$$

where we have taken into account that the temporal behavior of all fields is proportional to $e^{-i\omega t}$ with angular frequency ω. Knowing both the electric and the magnetic field, the time-averaged energy flux per area per time is given by Poynting's vector [Eq. (14)]:

$$\mathbf{P} = \frac{c}{8\pi}\Re,(\mathbf{E}\times\mathbf{B}^*) \tag{14}$$

where the star superscript denotes complex conjugation. Thus, the total energy flux S per time emitted by the dipole emitter can be found by integrating **P** over two horizontal infinite planes inside the cavity. The planes enclose the emitter on both sides. Because the cavity is filled, by definition, with a non-absorbing solvent with a real-valued refractive index n, this integral is indeed equal to the total energy emitted by the dipole per time. It is important to note that S is a function of the angle θ between the dipole axis and the optical axis (perpendicular to the cavity surfaces), but does not depend on the azimuthal angle of the dipole orientation (angle around the optical axis). More specifically, when inserting Equations (2) and (13) into Equation (14), and after some algebra, one finds that [Eq. (15)]:

$$S(\theta,z_m) = S_\perp(z_m)\cos^2\theta + S_\parallel(z_m)\sin^2\theta \tag{15}$$

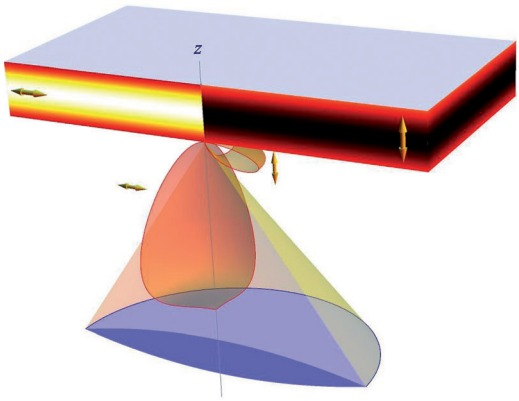

Figure 4. Geometry of the detection efficiency. The cavity strongly modifies the angular distribution of an emitting dipole inside the cavity as seen from the outside. Below the cavity, the angular distributions of emission for a horizontal (left side) and a vertical dipole (right side) positioned at the middle of the cavity are shown. The cone of light collection of the microscope objective is also shown. The detection is found by integrating the angular distribution of emission over the solid angle of this cone of light collection. The resulting detection efficiencies for a horizontal and vertical dipole as a function of vertical position are displayed as density plots inside the cavity. The cavity parameters and objective's numerical aperture are the same as for Figure 1.

where the $S_\perp$ and $S_\parallel$ are only functions of dipole position but not orientation. For a given cavity geometry and dielectric constants, the functions $S_{\perp,\parallel}$ themselves have to be calculated numerically. As an example, Figure 4 shows the behavior of $S_{\perp,\parallel}$ for a cavity composed of two silver-coated glass slabs for a dipole emitting at a wavelength of 670 nm.

Within the semi-classical picture of fluorescence emission, the radiative transition rate from the excited to the ground state of a fluorescing molecule is directly proportional to the energy flux S. Since we are interested in the relative enhancement (or damping) of this transition rate by the cavity, we have to compare S with the energy flux S_0 of the emitter in homogeneous solvent-filled space. In the normalization of Equation (9), this flux is given by Equation (16):

$$S_0 = \frac{cnp^2}{3} \tag{16}$$

2.3. Molecule Detection Function

The molecule detection function can be calculated following a similar strategy to that used when calculating the excitation intensity distribution. First, the electromagnetic field of the emitting dipole with given position and orientation is expanded into a plane wave representation [Eq. (2)] and then the transmission of each plane wave from inside the cavity to the outside is calculated. Although fluorescence detection is performed with a confocal microscope, the cavity height (~50 nm to 200 nm) and laser focus diameter (~300 nm) define such a small excitation volume that all the fluorescence that is collected by the objective also passes through the confocal aperture of the confocal microscope and is afterwards detected by the photodetector. This simplifies the calculation of the detection efficiency significantly, as it is then only a function of the vertical position of the emitting dipole and its orientation, but not its lateral position.

Outside the cavity, the electric field can be represented by a plane wave expansion similar to Equation (2), but with the reflection coefficients replaced by the appropriate transmission coefficients coupling the plane wave components of the emitting dipole inside the cavity to the corresponding plane wave components outside the cavity. Each plane wave component in such a representation corresponds to radiation (energy transport) into a certain direction in the far field. Moreover, because only plane wave components with purely imaginary exponents contribute to the far-field emission, one has to consider only components with $|\mathbf{q}| \leq nk_0$. Without loss of generality, let us consider a dipole with amplitude vector $\mathbf{p} = p_\parallel \mathbf{e}_x + p_\perp \mathbf{e}_z$, where $\mathbf{e}_x$ is the unit vector along the direction $\phi = 0$. Then the electric field amplitude of the plane wave components with their wave vectors within a solid-angle element $\sin\chi d\chi d\psi$, where χ and ψ are the polar and azimuthal propagation angles, are given by Equation (17):

$$\mathbf{E}_{\text{out}}(\chi,\psi) = p_\perp \mathbf{e}_p E_p^\perp(\chi) + p_\parallel \mathbf{e}_p E_p^\parallel(\chi)\cos\psi + p_\parallel \mathbf{e}_s E_s^\parallel(\chi)\sin\psi \tag{17}$$

where the χ-dependent functions are given by Equation (18):

$$\begin{aligned} E_p^\perp(\chi) &= \frac{nwq}{n_m w_m} \cdot \frac{t_p^- e^{iw_m z_m} + t_p^- r_p^+ e^{iw_m(2h-z_m)}}{1 - r_p^+ r_p^- e^{2iw_m h}} \\ E_p^\parallel(\chi) &= \frac{nw}{n_m} \cdot \frac{t_p^- e^{iw_m z_m} - t_p^- r_p^+ e^{iw_m(2h-z_m)}}{1 - r_p^+ r_p^- e^{2iw_m h}} \\ E_s^\parallel(\chi) &= \frac{nw}{w_m} \cdot \frac{t_s^- e^{iw_m z_m} + t_s^- r_s^+ e^{iw_m(2h-z_m)}}{1 - r_s^+ r_s^- e^{2iw_m h}} \end{aligned} \tag{18}$$

where $t_{p,s}^-$ is Fresnel's transmission coefficients for the transmission of plane waves from the inside to the outside through the bottom of the cavity. Each of the plane wave components as given by Equation (17) is connected with an energy flux that is $cn/8\pi$ times the absolute square amplitude of the electric field vector. By integrating this energy flux over the objective's solid angle of light collection, one obtains the total energy flux captured by the detection. Similar to the total energy flux emitted by the dipole (see Section 2.2), the energy flux collected by the objective can also be cast into the form given by Equation (19):

$$S_{\text{det}}(\theta, z_m) = S_{\text{det},\perp}(z_m)\cos^2\theta + S_{\text{det},\parallel}(z_m)\sin^2\theta \tag{19}$$

The molecule detection function $u(\theta, z_m)$ of detecting a photon from a molecule with given dipole orientation θ and vertical position z_m is finally given as the ratio of that energy flux S_{det} and the total energy emission S as calculated in the previous section, that is, by Equation (20):

$$u(\theta, z_m) = \frac{S_{\text{det},\perp}\cos^2\theta + S_{\text{det},\parallel}\sin^2\theta}{S_\perp \cos^2\theta + S_\parallel \sin^2\theta} \tag{20}$$

The most significant cause for the sensitivity to molecular orientation of the detection efficiency is the strongly orientation-dependent angular distribution of radiation of the emitters, which is collected differently by detection optics with finite apertures. This is visualized in Figure 4, showing the angular distribution of radiation outside the cavity, together with the objective's cone light detection, as generated by a horizontally and by a vertically oriented dipole, respectively. Figure 4 also shows the molecule detection function inside the cavity for both dipole orientations for a cavity of same size and parameters as in Figure 1, but for an emission wavelength of 670 nm.

Finally, it should be mentioned that in ref. [30], we approximated the molecule detection function by Equation (21):

$$u(\theta, z_m) = \frac{S_{\text{det},\perp}}{S_\perp}\cos^2\theta + \frac{S_{\text{det},\parallel}}{S_\parallel}\sin^2\theta \tag{21}$$

which significantly simplifies the subsequent algebra, but which represents only a rough approximation of the exact relation of Equation (20). Therefore, in the present paper, we used the exact expression, as given by Equation (20).

2.4. Spectral Dispersion and Quantum Yield

So far we have considered all emission properties for a monochromatic emitter only. However, real fluorescent emitters have rather broad emission spectra, which one should take into account. In connection with the strong optical dispersion of metals, the derived expressions for the emission rate S and molecule detection function u will also be wavelength-dependent, that is, $S=S(\theta,z_m,\lambda)$ and $u=u(\theta,z_m,\lambda)$. Next, our calculations of S considered only the radiative energy emission of an electric dipole. Actual molecules have both radiative and non-radiative emission channels. Then, the total deexcitation rate $k(\theta,z_m,\lambda)$ is given by Equation (22):

$$k(\theta,z_m,\lambda) = k_\perp(z_m,\lambda)\cos^2\theta + k_\parallel(z_m,\lambda)\sin^2\theta \tag{22}$$

where $k_{\parallel,\perp}(z_m,\lambda)$ is given by Equation (23):

$$k_{\parallel,\perp}(z_m,\lambda) = k_{nr} + \frac{S_{\parallel,\perp}(z_m,\lambda)}{S_0}k_{rad} = \frac{1}{\tau_0}\left(1-\Phi+\frac{S_{\parallel,\perp}(z_m,\lambda)}{S_0}\Phi\right) \tag{23}$$

Here, k_{nr} denotes the non-radiative deexcitation rate, $\tau_0=(k_{nr}+k_{rad})^{-1}$ the free-space lifetime, and Φ the fluorescence quantum yield. We have silently assumed that the free-space emission rate S_0 is independent on wavelength, thus neglecting optical dispersion of the solvent. The total deexcitation rate over the whole emission spectrum is then given by the weighted average [Eq. (24)]:

$$K(\theta,z_m) = \langle k(\theta,z_m,\lambda)\rangle_\lambda = \frac{\int k(\theta,z_m,\lambda)F_0(\lambda)d\lambda}{\int F_0(\lambda)d\lambda} \tag{24}$$

where $F_0(\lambda)$ is the emission spectrum of the dye in free solution, which is proportional to the chance that an excited molecule emits a photon at wavelength λ if there is no cavity present.

2.5. Rotational Diffusion

The next complication stems from the fact that molecules in solution often exhibit fast rotational diffusion, on a timescale similar to that of their excited state lifetimes. In that case, the molecules experience a rapidly fluctuating local mode density, and the observable emission rate will differ from that of dipoles with fixed orientation. We have only recently solved this problem in ref. [30]. Let us consider an ensemble of molecules which had been excited by a short laser pulse into their excited state. As we have seen above, these molecules will exhibit a deexcitation rate K that depends on their vertical position z_m within the cavity, and on the angle θ between their emission dipole axis and the vertical. The probability density $p(\theta,t)$ to find a molecule still in its excited state at time t with orientation angle θ obeys the following rotational diffusion equation [Eq. (25)]:

$$\frac{\partial p(\theta,z_m,t)}{\partial t} = \frac{D}{\sin\theta}\frac{\partial}{\partial\theta}\sin\theta\frac{\partial p(\theta,z_m,t)}{\partial\theta} - K(\theta,z_m)(\theta,t) \tag{25}$$

where the first term on the right-hand side is the rotational diffusion operator[38] multiplied with the rotational diffusion coefficient D, and the second term accounts for deexcitation. The initial distribution $p(\theta,t=0)$ right after excitation is defined by the polarization and intensity of the focused excitation light by means of Equation (26):

$$p(\theta,z_m,t=0) = \frac{3\left(I_\perp\cos^2\theta + I_\parallel\sin^2\theta\right)}{2\left(I_\perp+2I_\parallel\right)} \tag{26}$$

Next, the solution of Equation (25) can be found by expanding $p(\theta,t)$ into a series of Legendre polynomials $P_\ell(\cos\theta)$, as given by Equation (27):

$$p(\theta,z_m,t) = \sum_\ell^\infty a_\ell(z_m,t)P_\ell(\cos\theta) \tag{27}$$

where $a_\ell(t)$ denotes time-dependent expansion coefficients. Inserting that into Equation (25) yields an infinite set of ordinary differential equations for $a_\ell(t)$ [Eq. (28)]:

$$\frac{da_\ell(z_m,t)}{dt} = -D\ell(\ell+1)a_\ell(z_m,t) - \sum_{\ell'}M_{\ell\ell'}a_{\ell'}(z_m,t) \tag{28}$$

where the transition matrix $M_{\ell\ell'}$ is defined by the integrals given by Equation (29):

$$M_{\ell\ell'} = \frac{2\ell+1}{2}\int_{-1}^{1}dxP_\ell(x)P_{\ell'}(x)\left(x^2\Delta K + K_\parallel\right) \tag{29}$$

with the abbreviations $K_{\perp,\parallel}=\langle k_{\perp,\parallel}(z_m,\lambda)\rangle_\lambda$, and $\Delta K=K_\perp-K_\parallel$. By carrying out the integration, one finds that the only non-vanishing components of $M_{\ell\ell'}$ are given by Equation (30):

$$M_{\ell\ell'} = \begin{cases} \frac{(\ell-1)\ell}{(2\ell-3)(2\ell-1)}\Delta K & \text{for} \quad \ell'=\ell-2 \\ \frac{2\ell(\ell+1)-1}{(2\ell-1)(2\ell+3)}\Delta K + K_\parallel & \text{for} \quad \ell'=\ell \\ \frac{(\ell+1)(\ell+2)}{(2\ell+3)(2\ell+5)}\Delta K & \text{for} \quad \ell'=\ell+2 \end{cases} \tag{30}$$

From the initial condition, Equation (26), one finds that the only non-vanishing initial values a_ℓ are [Eq. (31)]:

$$\begin{aligned} a_0(t=0) &= \frac{1}{2} \\ a_2(t=0) &= \frac{I_\perp - I_\parallel}{I_\perp + 2I_\parallel} \end{aligned} \tag{31}$$

Although Equation (28) represents an infinite set of differential equations, it occurs that for our experimental conditions a truncation of the series expansion of Equation (27) at a maximum value $\ell_{max}=10$ yields an accurate solution to the problem that does not change when further increasing this truncation value.

2.6. Observable Average Lifetime

It remains to find an expression for the observable fluorescence intensity as a function of time after the excitation pulse. This is given by Equation (32):

$$I(t) = \int_0^h dz_m \int_0^\pi \sin\theta p(\theta, z_m, t)\langle k(\theta, z_m, \lambda)u(\theta, z_m, \lambda)\rangle_\lambda \qquad (32)$$

where $\langle\rangle_\lambda$ again denotes the weighted average over all wavelengths as defined in Equation (24). Finally, the observable mean fluorescence lifetime $\langle\tau\rangle$ is found as Equation (33):

$$\langle\tau\rangle = \int_0^\infty dt I(t)t \Big/ \int_0^\infty dt I(t) \qquad (33)$$

which is exactly the function used for fitting the experimentally determined lifetime values.

Experimental Section

A schematic of the experimental setup is shown in Figure 5. A homemade nanocavity consists of two silver mirrors placed at subwavelength distance one from each other. The bottom silver mirror (35 nm thick) was prepared by vapor deposition onto a cleaned glass cover slide (thickness 170 m) using an electron beam source (Univex 350, Laybold) under high-vacuum conditions

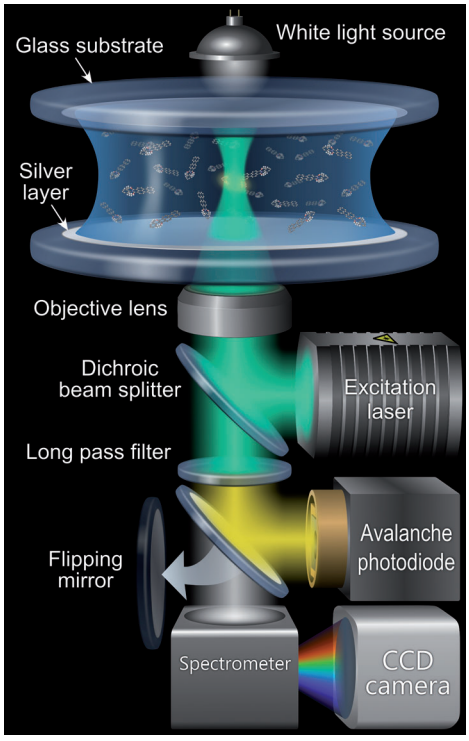

Figure 5. Experimental setup. The nanocavity consists of two silver layers, deposited on the glass surface. The upper silver layer is sputtered on the surface of a plano-convex lens, which allows one to tune the cavity length by moving the cavity in a horizontal plane. It should be noted that within the focal spot of a diffraction-limited objective lens focal spot, the cavity acts as a plane-parallel resonator.

($\sim 10^{-6}$ mbar). The top silver layer (75 nm thick) was prepared by vapor deposition of silver on the surface of a plan-convex lens (focal length of 150 mm) under the same conditions. During vapor deposition, film thickness was monitored using an oscillating quartz unit, and afterwards verified by atomic force microscopy measurements. The complex-valued wavelength-dependent dielectric constants of the silver films were determined by ellipsometry (Nanofilm ep3, Accurion GmbH, Göttingen). The cavity length was determined by measuring the white-light transmission spectrum[26,28] using a spectrograph (SR 303i, Andor) and a CCD camera (iXon DU897 BV, Andor).

For the QY measurements, a droplet of a micromolar solution of dye molecules in water (either rhodamine 6G, OregonGreen 488, Alexa 488, or Atto 488) was placed between the cavity mirrors. For fluorescein, we used a 0.1 N aqueous sodium hydroxide solution. Fluorescence lifetime measurements were performed with a home-built confocal microscope equipped with a high numerical aperture objective (UPLSAPO, 60×, N.A. = 1.2 water immersion, Olympus). A white-light laser system (SC400-4-80, Fianium) with an acousto-optical tunable filter (AOTFnC-400.650-TN, AA Optic) served as the excitation source ($\lambda_{exc} = 488$ nm). The excitation light was reflected by a dichroic mirror (BrightLine FF484-FDi01, Semrock) towards the objective. Back-scattered excitation light was blocked with a long-pass filter (EdgeBasic BLP01-488R, Semrock). Collected fluorescence was focused onto the active area of a single-photon detection module (PDM series, MPD). Data acquisition was accomplished with a multichannel picosecond event timer (HydraHarp 400, PicoQuant GmbH). Photon arrival times were histogrammed (bin width 50 ps) for obtaining fluorescence decay curves, and all curves were recorded until reaching at least 10^4 counts at maximum. The fluorescence decay curves were fitted with a multi-exponential decay model, from which the average excited state lifetime was calculated. Positioning of the focal spot inside the cavity was done by moving the sample with a piezo nano-positioning stage PI P-562.

3. Results and discussion

After placing a 10 microliter droplet of a micromolar solution of dye between the cavity mirrors, we recorded fluorescence decay curves for a series of values of cavity length. The spherical shape of the upper mirror allowed us to reversibly tune the cavity length by moving the cavity laterally with respect to the excitation focus with the piezo nano-positioning stage. It should be noted that across the excitation focus, the cavity can be considered as a plane-parallel resonator.[26] To exclude any influence of potential mechanical instabilities of the cavity on the obtained results, we recorded white-light transmission spectra of the cavity before and after acquiring each fluorescence decay curve. By fitting the white-light transmission curves we determined exact value of the cavity geometry. For doing that we had to know the exact values of the wavelength-dependent complex-valued refractive index of the silver layers, which we determined by ellipsometry measurements.

Acquisition of fluorescence decay curves was done in the range of white-light transmission maxima between 500 and 650 nm, corresponding to the fluorescence emission bands of the selected dyes. Figure 6 shows the results of the measurements for rhodamine 6G, Alexa 488, Oregon Green 488, Atto 488, and fluorescein (red circles) as a function of maxi-

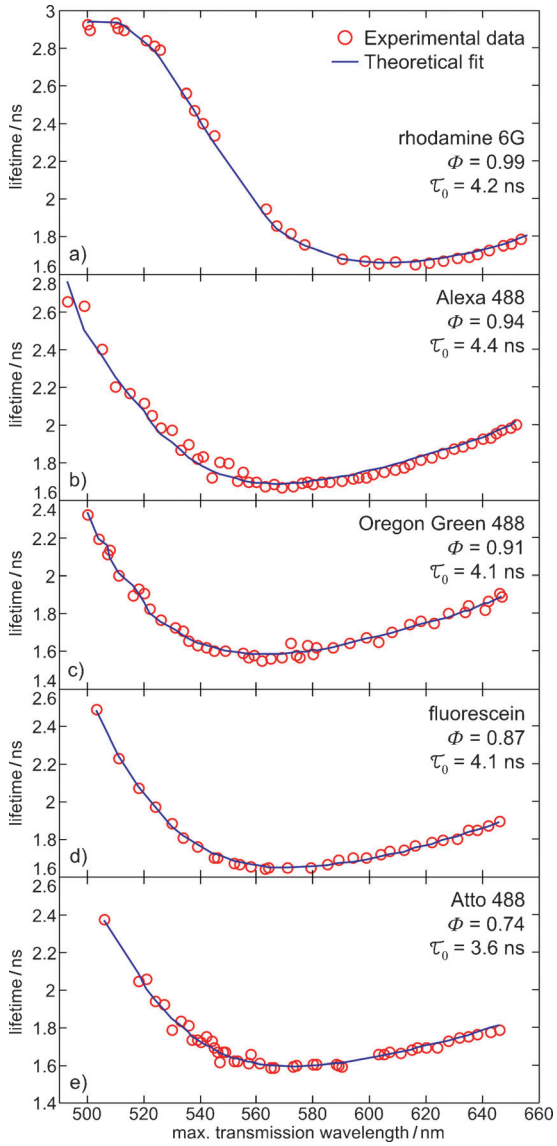

Figure 6. Cavity-controlled fluorescence lifetime of a rhodamine 6G, Alexa 488, OregonGreen 488 and Atto 488 in water and fluorescein in 0.1 N NaOH aqueous solution as a function of the maximum transmission wavelength of the resonator, which is linearly proportional to the cavity length. Red circles are the experimental data, blue curves are fits of the model. Φ and τ_0 indicate the values of the QY and free space fluorescence lifetime, respectively.

mum transmission wavelength, which is linearly proportional to the cavity length. The curves show a strong, dye-specific decrease of the lifetime values with increasing cavity length. The solid lines show fits of the theoretical model to the experimental data, where the only free fit parameters were the free space lifetime τ_0, and the fluorescence QY value Φ. In the model calculations, we assumed that the rotational diffusion time is much faster than the fluorescence decay time, which is justified for small dyes in aqueous solutions.[30] Table 1 displays the determined values of fluorescence lifetime and QY and compares them with literature values. For determining the errors of our nanocavity measurement method, we employed Efron's bootstrap algorithm.[40]

Table 1. Values of the fluorescence quantum yield Φ_{meas} and free space lifetimes τ_{meas} of measured dyes, compared to the literature values (Φ_{lit} and τ_{lit}).

	Φ_{meas}	Φ_{lit}	τ_{meas} [ns]	τ_{lit} [ns]
Rhodamine 6G	0.99 ± 0.03	0.89–1[1,11,41–44]	4.2 ± 0.3	4.1[1,45]
Fluorescein[a]	0.87 ± 0.02	0.79–0.95[1,8,13,43,46]	4.1 ± 0.2	4.0[1]
Alexa 488	0.94 ± 0.05	0.92[47]	4.4 ± 0.4	4.1[47]
Oregon Green 488	0.91 ± 0.05	~0.90[48]	4.1 ± 0.4	4.1[48]
Atto 488	0.74 ± 0.06	0.80[49]	3.6 ± 0.4	3.2[49]

[a] in 0.1 N NaOH aqueous solution.

As can be seen in Table 1, the error values of the QY measurements do not exceed 0.06 and can be as small as 0.02. As all measurements were performed by using only a 10 microliter droplet of a micromolar solution, the precision of the nanocavity-based method exceeds, to our knowledge, the precision of all other existing QY determination techniques. Moreover, the excellent agreement between our measurements and the literature values demonstrates the reliability of the nanocavity-based method. Since the amplitude of the chromophore's cavity-induced radiative rate modification is proportional to the quantum yield, the precision of the nanocavity-based method will decrease for dyes of low quantum yield, compared to the values obtained in this work.

4. Conclusions

We presented a novel method for measuring absolute values of the photoluminescence QY using a metal nanocavity. By recording fluorescence lifetime curves of molecules at different values of cavity length, we extracted both the free space fluorescence lifetime and the QY values. The excellent agreement between the experimental QY data with the literature values demonstrates the accuracy and precision of our method. The small size and simplicity of the nanocavity construction allows its use with any standard confocal fluorescence microscope equipped with a spectrometer and a time-correlated single-photon counting extension for lifetime measurements. Thus, measurements of QY values for any kind of fluorophore can easily be realized. This can also include QY measurements on unconventional types of emitters such as semiconductor nanocrystals, nanodiamonds, or carbon nanotubes.

Acknowledgement

Financial support by the Deutsche Forschungsgemeinschaft is gratefully acknowledged (SFB 937, project A5 and SFB 803, project A10). A.I.C. thanks the Alexander von Humboldt Foundation for financial support.

Keywords: cavities · confocal microscopy · nano-optics · quantum yields · radiative rates

[1] J. R. Lakowicz, *Principles of Fluorescence Spectroscopy, 3rd ed.*, Springer, New York, **2006**.
[2] S. Reineke, F. Lindner, G. Schwartz, N. Seidler, K. Walzer, B. Lüssem, K. Leo, *Nature* **2009**, *459*, 234 – 239.
[3] B. Lounis, W. E. Moerner, *Nature* **2000**, *407*, 491 – 493.
[4] B. C. Thompson, J. M. J. Frechet, *Angew. Chem.* **2008**, *120*, 62 – 82; *Angew. Chem. Int. Ed.* **2008**, *47*, 58 – 77.
[5] N. Tessler, *Adv. Mater.* **1999**, *11*, 363 – 370.
[6] I. L. Medintz, H. H. Uyeda, E. R. Goldman, H. Mattoussi, *Nat. Mater.* **2005**, *4*, 435 – 446.
[7] S. I. Vavilov, *Z. Phys.* **1924**, *22*, 266 – 272.
[8] J. N. Demas, G. A. Crosby, *J. Phys. Chem.* **1971**, *75*, 991 – 1024.
[9] J. N. Demas, *Measurement of Photon Yields*, Academic Press, New York, **1982**.
[10] U. Resch-Genger, K. Hoffmann, W. Nietfeld, A. Engel, J. Neukammer, R. Nitschke, B. Ebert, R. Macdonald, *J. Fluoresc.* **2005**, *15*, 337 – 362.
[11] C. Würth, M. Grabolle, J. Pauli, M. Spieles, U. Resch-Genger, *Anal. Chem.* **2011**, *83*, 3431 – 3439.
[12] J. P. Gordon, R. C. C. Leite, R. S. Moore, S. P. Porto, J. R. Whinnery, *J. Appl. Phys.* **1965**, *36*, 3.
[13] E. H. Brannon, D. J. Magde, *J. Phys. Chem.* **1978**, *82*, 705 – 709.
[14] J. C. de Mello, H. F. Wittmann, R. H. Friend, *Adv. Mater.* **1997**, *9*, 230 – 232.
[15] C. Würth, C. Lochmann, M. Spieles, J. Pauli, K. Hoffmann, T. Schüttrigkeit, T. Franzl, U. Resch-Genger, *Appl. Spectrosc.* **2010**, *64*, 733 – 741.
[16] E. M. Purcell, *Phys. Rev.* **1946**, *69*, 681.
[17] M. Ringler, A. Schwemer, M. Wunderlich, A. Nichtl, K. Kürzinger, T. A. Klar, J. Feldmann, *Phys. Rev. Lett.* **2008**, *100*, 203002.
[18] J. Macklin, J. Trautman, T. Harris, L. Brus, *Science* **1996**, *272*, 255 – 258.
[19] X. Brokmann, L. Coolen, M. Dahan, J. P. Hermier, *Phys. Rev. Lett.* **2004**, *93*, 107403.
[20] K. H. Drexhage, *Prog. Opt.* **1974**, *12*, 163.
[21] B. C. Buchler, T. Kalkbrenner, C. Hettich, V. Sandoghdar, *Phys. Rev. Lett.* **2005**, *95*, 063003.
[22] Y. Cesa, C. Blum, J. M. van den Broek, A. P. Mosk, W. L. Vos, V. Subramaniam, *Phys. Chem. Chem. Phys.* **2009**, *11*, 2525 – 2531.
[23] W. P. Ambrose, P. M. Goodwin, J. C. Martin, R. A. Keller, *Science* **1994**, *265*, 364 – 367.
[24] W. Trabesinger, A. Kramer, M. Kreiter, B. Hecht, U. P. Wild, *Appl. Phys. Lett.* **2002**, *81*, 2118 – 2120.
[25] K. J. Vahala, *Nature* **2003**, *424*, 839 – 846.
[26] M. Steiner, F. Schleifenbaum, C. Stupperich, A. V. Failla, A. Hartschuh, A. J. Meixner, *ChemPhysChem* **2005**, *6*, 2190 – 2196.
[27] A. Chizhik, F. Schleifenbaum, R. Gutbrod, A. Chizhik, D. Khoptyar, A. J. Meixner, J. Enderlein, *Phys. Rev. Lett.* **2009**, *102*, 073002.
[28] A. I. Chizhik, A. M. Chizhik, D. Khoptyar, S. Bär, A. J. Meixner, J. Enderlein, *Nano Lett.* **2011**, *11*, 1700 – 1703.
[29] A. I. Chizhik, A. M. Chizhik, A. M. Kern, T. Schmidt, K. Potrick, F. Huisken, A. J. Meixner, *Phys. Rev. Lett.* **2012**, *109*, 223902.
[30] A. I. Chizhik, I. Gregor, F. Schleifenbaum, C. B. Müller, C. Röling, A. J. Meixner, J. Enderlein, *Phys. Rev. Lett.* **2012**, *108*, 163002.
[31] E. Fermi, *Rev. Mod. Phys.* **1932**, *4*, 87.
[32] E. Wolf, *Proc. R. Soc. London Ser. A* **1959**, *253*, 349 – 357.
[33] B. Richards, E. Wolf, *Proc. R. Soc. London Ser. A* **1959**, *253*, 358 – 379.
[34] H. Weyl, *Ann. Phys.* **1919**, *365*, 481 – 500.
[35] J. Enderlein, T. Ruckstuhl, S. Seeger, *Appl. Opt.* **1999**, *38*, 724 – 732.
[36] F. Abelès, *J. Phys. Radium* **1950**, *11*, 307 – 310.
[37] O. S. Heavens, *Optical Properties of Thin Films*, Butterworth, London, **1955**.
[38] B. J. Berne, R. Pecora, *Dynamic Light Scattering: With Applications to Chemistry, Biology, and Physics*, Dover, **2000**.
[39] R. R. Chance, A. Prock, R. Silbey, *Adv. Chem. Phys.* **1978**, *37*, 1 – 65.
[40] B. Efron, *Ann. Stat.* **1979**, *7*, 1 – 26.
[41] L. Porrès, A. Holland, L.-O. Pålsson, A. P. Monkman, C. Kemp, A. Beeby, *J. Fluoresc.* **2006**, *16*, 267 – 273.
[42] J. Arden, G. Deltau, V. Huth, U. Kringel, D. Peros, K. H. Drexhage, *J. Lumin.* **1991**, *48/49*, 352 – 358.
[43] R. E. Kellogg, R. G. Bennett, *J. Chem. Phys.* **1964**, *41*, 3042 – 3045.
[44] R. F. Kubin, A. N. Fletcher, *J. Lumin.* **1982**, *27*, 455 – 462.
[45] D. Magde, G. E. Rojas, P. Seybold, *Photochem. Photobiol.* **1999**, *70*, 737 – 744.
[46] G. Weber, F. W. J. Teale, *Trans. Faraday Soc.* **1957**, *53*, 646 – 655.
[47] http://de-de.invitrogen.com/site/de/de/home/References/Molecular-Probes-The-Handbook/tables/Fluorescence-quantum-yields-and-life-times-for-Alexa-Fluor-dyes.html.
[48] R. P. Haughland, *Handbook of Fluorescent Probes and Research Products, 11th ed.*, Molecular Probes, **2010**.
[49] https://www.atto-tec.com.

Received: November 12, 2012
Published online on January 18, 2013